Volume 1 | Number 1 | Jan 2013 | Pages 1–100

Nanoscale

www.rsc.org/nanoscale

Nanoscale

PAPER

High performance triboelectric nanogenerator for self-powered non-volatile ferroelectric transistor memory

Huajing Fang,[a] Qiang Li,[a] Wenhui He,[a] Jing Li,[a] Qingtang Xue,[b] Chao Xu,[a] Lijing Zhang,[a] Tianling Ren,[b] Guifang Dong,[a] H.L.W. Chan,[c] Jiyan Dai*[c] and Qingfeng Yan*[a]

We demonstrate an integrated module of self-powered ferroelectric transistor memory based on the combination of ferroelectric FET and triboelectric nanogenerator (TENG). The novel TENG was made of self-assembled polystyrene nanospheres array and poly(vinylidene fluoride) porous film. Owing to this unique structure, it exhibits an outstanding performance with the output voltage as high as 220 V per cycle. Meanwhile, the arch-shaped TENG is shown to be able to pole a bulk ferroelectric $0.65Pb(Mg_{1/3}Nb_{2/3})O_3$-$0.35PbTiO_3$ (PMN-PT) single crystal directly. Based on this effect, a bottom gate ferroelectric FET was fabricated using pentacene as channel material and PMN-PT single crystal as gate insulator. Systematic tests illustrate that the ON/OFF current ratio of this transistor memory is approximately 10^3. More importantly, we demonstrate the feasibility to switch the polarization state of this FET gate insulator, namely the stored information, by finger tapping the TENG with a designed circuit. These results may open up a novel application of TENGs in the field of self-powered memory system.

Introduction

Harvesting clean and sustainable energy directly from the environment is one of the most promising approaches to meet rapidly increasing energy demands and control of environment pollution.[1-3] As tremendous amount of mechanical energy surrounding us are available around the clock, generators based on electromagnetic,[4,5] piezoelectric,[6,7] and electrostatic[8] effects have been widely employed to convert these mechanical energy into electricity. Recently, a new concept of nanogenerator which utilizes the well-known triboelectricfication and electrostatic induction phenomenon has been developed as an emerging technology. Since the first invention of the triboelectric nanogenerator (TENG) was reported in early 2012,[9] there have been rapid advances in this field. Many efforts have been made to improve the output performance of the TENG by material optimization,[10-12] advanced structural design, and others.[13-15] Among these, surface morphology of the friction layers has been demonstrated as a main factor to affect the TENG performance. So far, different preparation methods such as photolithography,[16] dry-etching,[17] anodic aluminum oxide template[18] and block copolymer self-assembly[19] have been used to fabricate micro/nanostructure pattern on the contact surface of TENG. However, most of these methods are difficult for mass production or rely on expensive equipment. As self-assembly of 2D colloidal crystals is an effective strategy for the fabrication of ordered nanostructures, it have drawn much attention in various applications for surface patterning due to the advantages of facile, inexpensive and repeatable.[20-25] In spite of their wide applications, 2D colloidal crystals have rarely been illustrated as a solution to improve the performance in triboelectric applications. In addition, enriching its functionality as self-powered device is another research direction of TENG. By using the nanogenerator as the power source, many actual applications such as UV sensors,[26] chemical sensors,[27] anticorrosion,[28] electrochromic device,[29] and trace memorization[30] have been successfully demonstrated.

On the other hand, a memory functionality is essential to many applications of electronic devices. Ferroelectric materials show a great potential as the information can be stored via two antiparallel polarization states interpreted as Boolean 0 or 1. High-performance non-volatile ferroelectric memories, in particular ferroelectric-gate field effect transistors (FETs) have attracted great attention because of their non-destructive memory operation through a semiconducting channel, scalable feature size and short program pulse width.[31-33] A variety of semiconducting materials such as MoS_2,[34] poly(3-hexylthiophene) (P3HT),[35] graphene,[36] single-walled carbon nanotube (SWCNT),[37] and pentacene[38] have been used to optimize the memory performance. The stored information of all these ferroelectric FETs is written by poling the ferroelectric insulator with a conventional gate voltage pulse. However, self-powered ferroelectric-FET has not been realized so far.

a. Department of Chemistry, Tsinghua University, Beijing, 100084, China. E-mail: yanqf@mail.tsinghua.edu.cn (Q. Yan)
b. Institute of Microelectronics, Tsinghua University, Beijing 100084, China.
c. Department of Applied Physics, The Hong Kong Polytechnic University, Hong Kong, China. E-mail: jiyan.dai@polyu.edu.hk (J. Y. Dai)
†Electronic Supplementary Information (ESI) available. See DOI: 10.1039/x0xx00000x

In this work, we demonstrate an integrated module of self-powered ferroelectric transistor memory based on the combination of ferroelectric FET and TENG. First, we have developed a simple and low-cost method to fabricate an arch-shaped TENG with two different nanostructures on each friction layer. The poly(vinylidene fluoride) (PVDF) porous film was deposited on a PET substrate by spin coating with an appropriate preparation. Large area polystyrene (PS) colloidal monolayer utilizing as the opposite material was achieved by assembling the colloidal nanospheres at the air/water interface and transferred to another PET substrate. The resultant TENG shows a high output voltage up to 220 V accompanied by outstanding stability over long period of measurement. Then, we present a new method to pole a perovskite ferroelectric crystal $0.65Pb(Mg_{1/3}Nb_{2/3})O_3$- $0.35PbTiO_3$ (PMN-PT) by taking advantage of the high voltage provided by our TENG. To the best of our knowledge, it is the first report about poling perovskite ferroelectric material by using the nanogenerator as a nonconventional source. The PMN-PT single crystal shows excellent piezoelectric properties after poling. With a designed circuit, the written process of the ferroelectric transistor memory can be easily realized by finger tapping the TENG. Our results may open up a novel application of TENGs in the field of self-powered memory system.

Experimental

Fabrication of TENG

The commercial ITO coated PET (Sigma-Aldrich) was cleaned by ethanol (99.95%, Sinopharm, China) and DI water (resistivity up to 18.2 MΩ•cm, Ultra-Pure UV, China) and used as the flexible substrate. PVDF powder with an average Mw of ~534000 and an average size of 200 nm was purchased from Sigma-Aldrich and used without any purification. All the other reagents were purchased from Sinopharm, China. 0.25g PVDF was mixed with 3ml DMF and 3ml acetone in a triangular flask. The solution was stirred at room temperature for 2h to dissolve PVDF completely. The porous film was prepared by spin-coating the PVDF solution on a piece of PET substrate and drying at 80 ^{o}C. Monodisperse PS colloidal spheres of 600 nm in diameter were synthesized through the emulsifier-free polymerization method.[39] After being washed with DI water, the PS nanospheres were self-assembled into monolayer colloidal crystals at the air/water interface. The floating monolayer colloidal crystals were then transferred to the PET substrate. The detailed synthesis and transfer methods can be referred to our earlier work.[40,41] To achieve an improved adhesion between the PS nanospheres and the PET substrate, the as-transferred PS colloidal monolayer was thermally annealed at 100 ^{o}C for 30 min. Then, the two parts described above were packaged together with face to face. The top and bottom ITO electrodes were wired out by an adhesive aluminum tape for device characterization.

Fabrication of ferroelectric-gate field effect transistor

The PMN-PT single crystal with composition close to the morphotropic phase boundary (MPB) was grown by a slow cooling method at our laboratory. A [001]-oriented specimen ($4\times3\times0.27$ mm^3) was processed for piezoelectric test after being poled by the high voltage pulse of TENG. The ferroelectric FET based on pentacene film was prepared by the following procedure. By thinning and polishing the PMN-PT single crystal, we can get a slice of 100 μm in thickness as the ferroelectric insulator. The gate electrode was prepared by Au coating on the bottom of the PMN-PT slice. A 50 nm-thick pentacene film was evaporated on the top of PMN-PT slice with a low deposition rate of 1.2 nm/min. To complete the FET structure, a Au film with a thickness of 45 nm was evaporated over the pentacene layer using a shadow mask as the drain and source electrodes. The channel length was 60 μm and the channel width was 1 mm.

Characterization

The surface morphology of the self-assembled PS colloidal spheres monolayer and the PVDF porous film were examined by the field-emission scanning electron microscopy (FESEM, JEOL JSM-6335F). The output signal of the arch-shaped TENG was recorded by the digital multimeter (RIGOL DM3068) under mechanical tapping. The crystal structures of PMN-PT single crystals have been characterized through X-ray diffraction (XRD, Bruker D8-Advance). The thickness electromechanical coupling coefficient (k_t) was measured from the resonant frequencies (f_r) and anti-resonant frequencies (f_a), with an impedance analyzer (Agilent 4294A) according to IEEE standards. The piezoelectric strain constant d_{33} was measured using a quasi-static piezo-d_{33} meter (ZJ-4A, Institute of Acoustics, Chinese Academy of Sciences, Beijing, China). Domain structures were investigated using a polarized light microscope (PLM, Jiangnan XJZ-6, China). The performances of the ferroelectric-gate field effect transistor were assessed through a semiconductor characterization system (Keithley 4200SCS) in air.

Results and discussion

The 3D structure of the TENG is schematically detailed in Fig. 1, where it can be seen that the demonstrated device is constituted by two plates. On the upper plate, a porous PVDF thin film is prepared by spin coating. PVDF is purposely chosen here for its advantages of concave surface and easy processing. On the lower plate, the PET substrate is covered by a monolayer PS colloidal crystal. The voltage generation mechanism of this arch-shaped TENG originates from the transient charge flows induced by the coupling of contact electrification and electrostatic induction effect between these two friction layers. The difference in the ability of trapping electrons between the PS and PVDF leads to electron transfer when the friction materials are in contact with each other. After electrons being injected to the surface of PVDF porous film, the positive charges will be generated on the surface of PS nanospheres array correspondingly. When a compressive stress is applied to the TENG, the potential of the upper electrode rises immediately due to the contact of negatively charged PVDF porous film with the positive charges on the PS

nanospheres array. Accordingly, the potential of the lower electrode drops. Thus, the resulting potential difference between the two electrodes drives the charge flow forward. When the applied force is released, the charges flow back to the original electrodes to reach an electrostatic equilibrium.
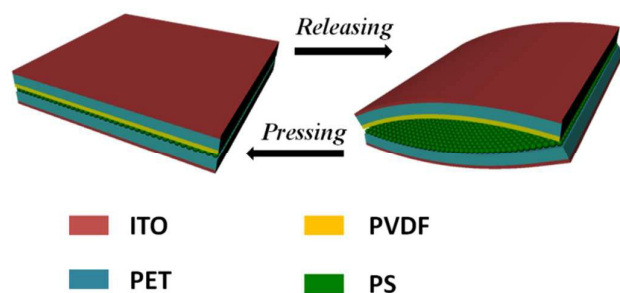
Fig. 1 Schematic 3D diagram depicting the structure and working mechanism of the arch-shaped triboelectric nanogenerator.

It has been demonstrated in previous works that micro/nanostructures existing on the surface of friction layers can contribute to higher performance of a TENG.[19] In our work, two different nanostructures are involved to enlarge the surface area and enhance the rubbing as well. The SEM image in Fig. 2a displays the morphology of the PS monolayer colloidal crystal obtained by self-assembly, where the diameter of the nanospheres is 600 nm. It is noteworthy that the PS nanospheres have sticked together to achieve a higher mechanical strength after thermal annealing. The surface morphology of PVDF porous film is shown in Fig. 2b. The PVDF nanostructures distributed on the PET substrate chaotically as the solvents evaporated rapidly after spin-coating.

Fig. 3a shows the open circuit voltage output from our arch-shaped TENG by vertically finger tapping, where it is apparent that the peak values of the voltage are approximately 220 V. To confirm the validity of the output signals, the TENG was measured under a reverse connection mode for the switching polarity test. As shown in Fig. 3b, the amplitudes of the output signals are almost the same as the ones we get under the forward connection, while the polarity is reversed. This phenomenon can prove that voltage signals are truly generated by the TENG. Furthermore, Fig. 3c shows the enlarged view of the output voltage over a single cycle, where one can see that the pulse width with the output voltage higher than 100 V is up to 2.7 ms. The power delivered from our TENG during one cycle of pressing and releasing motions is able to directly turn on 50 green LEDs without using any charging-discharging electric circuit (see ESI Video. 1†). Resistors were connected as external loads to further study the effective electric power of this TENG, the details can be found in ESI Fig. S1†. We also measured the response of output voltage to the tapping frequency, see ESI Fig. S2†. Long-term stability of the TENG was also examined by tapping the device vertically using a vibration exciter for sufficient cycles. The voltage amplitude is about 150 V under a given frequency of 3 Hz. The consistent output signals of the TENG are maintained over 1000

cycles without any performance degradation. These results distinctly confirm the mechanical stability and reproducibility of our TENG.
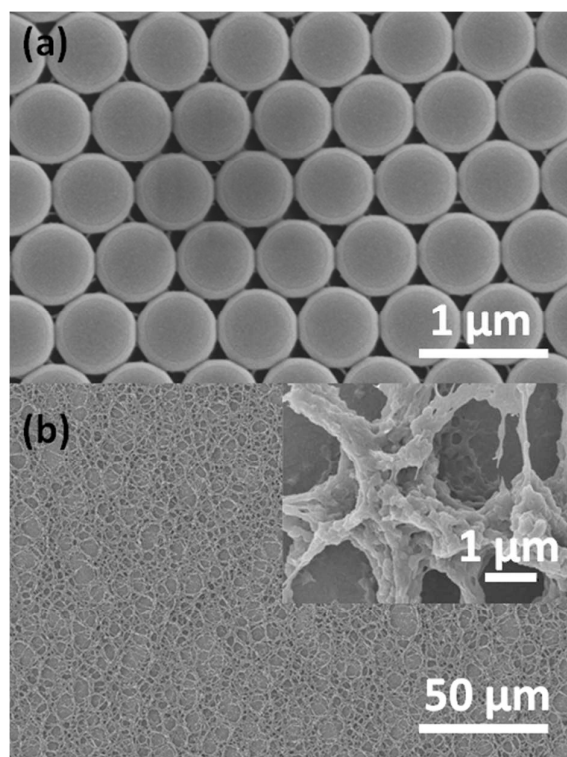
Fig. 2 SEM image of (a) PS nanospheres array and (b) PVDF porous film.
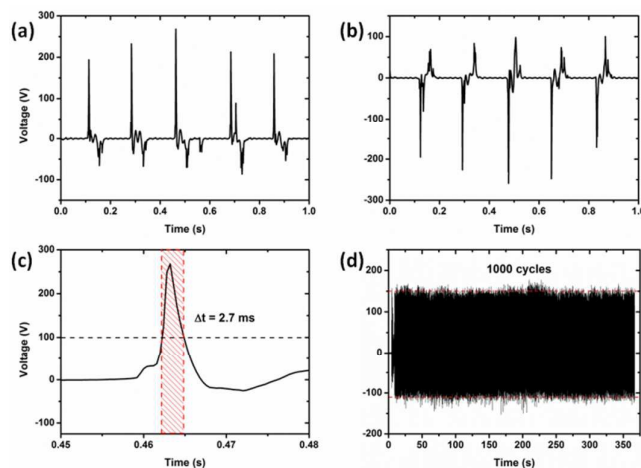
Fig. 3 (a) The open circuit output voltage signal of the TENG in forward connection during the finger tapping. (b) The open circuit output voltage signal of the TENG in reversed connection during the finger tapping. (c) The enlarged view of the output voltage generated by the TENG in the forward connection over a single tapping cycle. (d) Long-term stability test of the output voltage of the TENG under 3 Hz of continuous tapping for more than 1000 cycles, demonstrating the stability of the TENG.

PAPER   **Nanoscale**

The basic strategy for the nonconventional poling of ferroelectric materials is schematically shown in Fig. 4a. We connected the TENG to a [001]-oriented PMN-PT specimen (XRD pattern is shown in ESI Fig. S3†) through a bridge rectifier consisting of four diodes. The PMN-PT specimen was poled directly by the rectified output voltage pulse. (more details of the rectified output voltage are shown in ESI Fig. S4†) The thickness mode electromechanical coupling coefficient k_t is an important parameter for piezoelectric material after poling. It can be calculated as follow: [42]

$$k_t^2 = \frac{\pi}{2} \frac{f_r}{f_a} \tan(\frac{\pi}{2} \frac{f_a - f_r}{f_a})$$

The thickness mode resonance frequency (f_r) and the anti-resonance frequency (f_a) can be observed at 8.73 and 9.92 MHz in the impedance and phase spectra as shown in Fig. 4b, respectively. Thus, k_t is found to be 0.51, comparable to the value of PMN-PT crystal poled through a standard procedure.[43] Meanwhile, the piezoelectric strain constant d_{33} turns out to be 1040 pC/N when measured by a quasi-static piezo-d_{33} meter. Polarizing light microscopy observation of domain structure and extinction angle is an intuitive method to study the phase transition during the poling process.[44] Figs. 4c and 4d are the domain structures observed in the [001]-oriented PMN-PT crystal before and after poling by our TENG. The extinction angle of the domain structures in visual region is 0° (or 90°) under zero electric field. But the same region shows all angles extinction along [001] direction after applying a voltage pulse generated from the TENG. The total extinction indicates a quasi-single domain with tetragonal phase due to the dipoles rotation along the direction of pulse voltage. This extinction behavior in Fig. 4d indeed shows a significant difference compared to the fresh state in Fig. 4c, which implied that the crystal has been successfully poled. As we know, the polarization switching can occur in an order of 10^{-4} seconds with a sufficient electric field.[45] Thus, it comes naturally that ferroelectric materials with suitable thickness can be poled by the rectified output voltage pulses provided by the TENG.
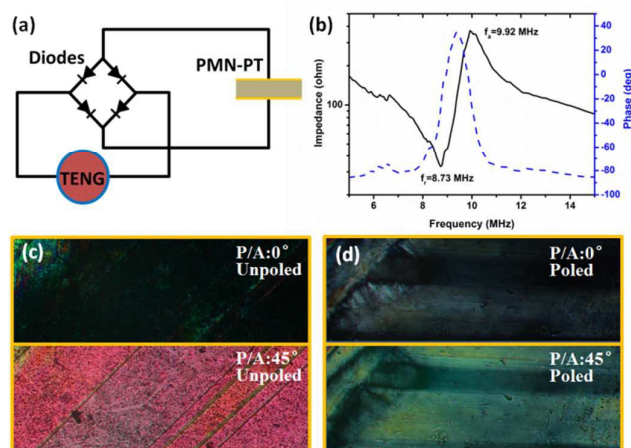
Fig. 4 (a) The bridge rectifier circuit diagram for poling the PMN-PT single crystal directly by the TENG. (b) The thickness mode impedance and phase spectra of the PMN-PT single crystal after poling. (c) Domain structures

observed in the [001] oriented PMN-PT crystal before poling. (d) Domain structures observed in the [001] oriented PMN-PT crystal after poling.
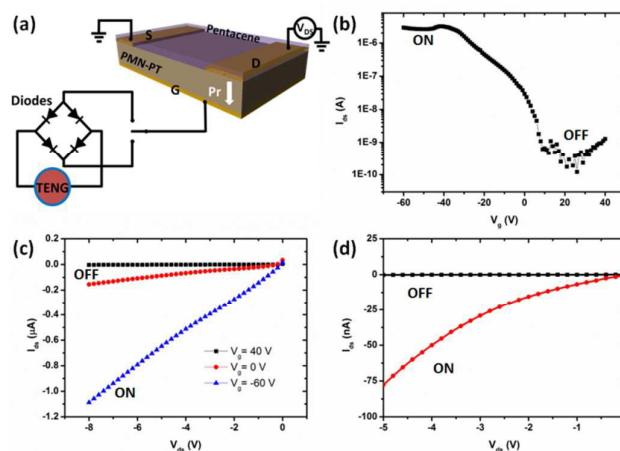
Fig. 5 Integration of the TENG device with a ferroelectric-gate field effect transistor to demonstrate a self-powered nonvolatile ferroelectric transistor memory. (a) Schematic illustration of the self-powered nanosystem. (b) The transfer curve of the pentacene ferroelectric transistors on sweeping the gate voltage from -60 V to 40 V under a V_{ds} of -8 V. (c) Typical I_{ds}-V_{ds} characteristics of a pentacene ferroelectric transistor with PMN-PT insulator. (d) Measurement of the I_{ds} upon applying a positive gate voltage pulse by the TENG (OFF state). The channel resistance decreases remarkably after application of a negative voltage pulse (ON state).

The above results provide an indication that it is possible to realize a polarization switching by the mechanical energy via the conversion of TENG. Inspired by these pioneer results, we have come up with the idea to integrate the TENG device with a ferroelectric-gate field effect transistor to demonstrate a self-powered non-volatile ferroelectric transistor memory. Fig. 5a schematically illustrates this self-powered nanosystem. The rectified output voltage pulse is applied on the ferroelectric transistor as a gate voltage to control the electric resistance of the channel. The binary state of resistance can be read out without alternative reversals of the ferroelectric polarization, as a non-volatile memory. The ferroelectric property of the PMN-PT slice used in this work has been characterized by P-E loops (ESI Fig. S5†). As we can see in Fig. S5, the remnant polarization P_r of the PMN-PT slice is 29 $\mu C/cm^2$. Such a large P_r enables the operation of our ferroelectric FET memory device. It can be seen from Fig. 5b, the ferroelectric-gate field effect transistor with pentacene channel exhibits p-type characteristics in the transfer curve (at a V_{ds} of -8 V) as the gate voltage sweeps from -60 to 40 V. The ratio of the corresponding ON (high) and OFF (low) channel current states is over 10^3, which allows for memory operation. Fig. 5c shows the typical I_{ds}-V_{ds} characteristics at different gate voltages. The I_{ds} is linearly proportional to V_{ds} in the low-voltage region, similar to that of a p-channel MIS FET fabricated using pentacene.[46] After the transistor is turned on, the I_{ds} increases rapidly with a negative bias in V_g owing to accumulation of excess holes in the pentacene channel. Thus, a subsequent application of a positive V_g larger than the coercive field of PMN-PT layer in principle can switch the polarization state,

leading to a remarkable decrease in the I_{ds}. To study the memory retention of this self-powered nanosystem, we applied the positive or negative writing pulse to the gate respectively by finger tapping the TENG. The I_{ds}-V_{ds} curves are shown in Fig. 5d. The black curve represents the OFF state after applying a positive gate pulse through the TENG. Conversely, the red curve corresponds to the ON state after applying a negative voltage pulse. The distinct bistable ON and OFF current states confirm the excellent memory operation. More efforts can be made to improve the performance of the ferroelectric FET. For instance, high density memory is one of the most pressing issues yet to be significantly addressed. This goal could possibly be achieved by scale-down of individual cell dimensions as well as material design including substitute the PMN-PT slice with thin film such as lead zirconatate titanate (PZT), $BaTiO_3$, even the PVDF-based organic ferroelectric polymer. Nevertheless, the TENG driven ferroelectric transistor memory described in this work has verified the feasibility to open up a new writing mode of memory devices.

Conclusions

In summary, we have successfully fabricated a new TENG consisting of self-assembled polystyrene nanospheres array and PVDF porous film as friction layers. The TENG shows a high output voltage up to 220 V accompanied by outstanding stability over long period of measurement. Furthermore, our work has demonstrated, for the first time, the possibility of nonconventional poling bulk ferroelectric materials with a TENG. Thus, the concept of self-powered non-volatile ferroelectric transistor memory has been realized by integrating the TENG device with a ferroelectric-gate field effect transistor. The method presented here provides a simple and potential approach of self-powered memory system.

Acknowledgements

Notes and references

1   S. Xu, Y. Qin, C. Xu, Y. G. Wei, R. S. Yang and Z. L. Wang, *Nat. Nanotechnology*, 2010, **5,** 366-373.
2   M. D. Han, X. S. Zhang, B. Meng, W. Liu, W. Tang, X. M. Sun, W. Wang and H. X. Zhang, *ACS Nano*, 2013, **7,** 8554-8560.
3   G. Zhu, J. Chen, T. Zhang, Q. Jing and Z. L. Wang, *Nat. Commun.*, 2014, **5,** 3426.
4   Y. C. Wu, X. Wang, Y. Yang and Z. L. Wang, *Nano Energy*, 2015, **11,** 162-170.
5   S. P. Beeby, R. N. Torah, M. J. Tudor, P. Glynne-Jones, T. O'Donnell, C. R. Saha and S. Roy, *J. Micromech. Microeng.*, 2007, **17,** 1257-1265.
6   S. Shin, Y. Kim, M. H. Lee, J. Jung and J. Nah, *ACS Nano*, 2014, **8,** 2766-2773.
7   S. Y. Xu, Y. W. Yeh, G. Poirier, M. C. McAlpine, R. A. Register and N. Yao, *Nano Lett.*, 2013, **13,** 2393-2398.
8   H. Tian, S. Ma, H. M. Zhao, C. Wu, J. Ge, D. Xie, Y. Yang and T. L. Ren, *Nanoscale*, 2013, **5,** 8951-8957.
9   F. R. Fan, Z. Q. Tian and Z. L. Wang, *Nano Energy*, 2012, **1,** 328-334.
10 S. Kim, M. K. Gupta, K. Y. Lee, A. Sohn, T. Y. Kim, K. S. Shin, D. Kim, S. K. Kim, K. H. Lee, H. J. Shin, D. W. Kim and S. W. Kim, *Adv. Mater.*, 2014, **26,** 3918-3925.
11 Z. H. Lin, G. Cheng, L. Lin, S. Lee and Z. L. Wang, *Angew. Chem., Int. Ed.*, 2013, **52,** 12545-12549.
12 S. H. Kwon, J. Park, W. K. Kim, Y. Yang, E. Lee, C. J. Han, S. Y. Park, J. Lee and Y. S. Kim, *Energy Environ. Sci.*, 2014, **7,** 3279-3283.
13 W. Q. Yang, J. Chen, Q. S. Jing, J. Yang, X. N. Wen, Y. J. Su, G. Zhu, P. Bai and Z. L. Wang, *Adv. Funct. Mater.*, 2014, **24,** 4090-4096.
14 P. Bai, G. Zhu, Z. H. Lin, Q. Jing, J. Chen, G. Zhang, J. Ma and Z. L. Wang, *ACS Nano*, 2013, 7, 3713-3719.
15 M. Taghavi, V. Mattoli, A. Sadeghi, B. Mazzolai and L. Beccai, *Adv. Energy Mater.*, 2014, **4,** 1400024.
16 S. H. Wang, L. Lin and Z. L. Wang, *Nano Lett.*, 2012, **12,** 6339-6346.
17 L. Lin, S. H. Wang, Y. N. Xie, Q. S. Jing, S. M. Niu, Y. F. Hu and Z. L. Wang, *Nano Lett.*, 2013, **13,** 2916-2923.
18 P. Bai, G. Zhu, Z. H. Lin, Q. Jing, J. Chen, G. Zhang, J. Ma and Z. L. Wang, *ACS Nano*, 2013, **7,** 3713-3719.
19 C. K. Jeong, K. M. Baek, S. Niu, T. W. Nam, Y. H. Hur, D. Y. Park, G. T. Hwang, M. Byun, Z. L. Wang, Y. S. Jung and K. J. Lee, *Nano Lett.*, 2014, **14,** 7031-7038.
20 M. Faustini, G. L. Drisko, A. A. Letailleur, R. S. Montiel, C. Boissière, A. Cattoni, A. M. Haghiri-Gosnet, G. Lerondel and D. Grosso, *Nanoscale*, 2013, **5,** 984-990.
21 T. Wang, X. Li, J. Zhang, Z. Ren, X. Zhang, X. Zhang, D. Zhu, Z. Wang, F. Han, X. Wang and B. Yang, *J. Mater. Chem.*, 2010, **20,** 152-158.
22 S. G. Jang, H. K. Yu, D. G. Choi and S. M. Yang, *Chem. Mater.*, 2006, **18,** 6103-6105.
23 Q. F. Yan, F. Liu, L. K. Wang, J. Y. Lee and X. S. Zhao, *J. Mater. Chem.*, 2006, **16,** 2132-2134.
24 X. Z. Ye and L. M. Qi, *Nano Today*, 2011, **6,** 608-631.
25 Y. Li, N. Koshizaki and W. P. Cai, *Coordin. Chem. Rev.*, 2011, **255,** 357-373.
26 Y. B. Zheng, L. Cheng, M. M. Yuan, Z. Wang, L. Zhang, Y. Qin and T. Jing, *Nanoscale*, 2014, **6,** 7842-7486.
27 Z. L. Wang, *ACS Nano*, 2013, **7,** 9533-9557.
28 Z. Wang, L. Cheng, Y. B. Zheng, Y. Qin and Z. L. Wang, *Nano Energy*, 2014, **10,** 37-43.
29 M. H. Yeh, L. Lin, P. K. Yang and Z. L. Wang, *ACS Nano*, 2015, **7,** 3713-3719.
30 X. Y. Chen, M. Iwamoto, Z. M. Shi, L. M. Zhang and Z. L. Wang, *Adv. Funct. Mater.*, 2015, **25,** 739-747.
31 A. K. Tripathi, A. J. J. M. van Breemen, J. Shen, Q. Gao, M. G. Ivan, K. Reimann, E. R. Meinders and G. H. Gelinck, *Adv. Mater.*, 2011, **23,** 4146-4151.
32 R. C. G. Naber, K. Asadi, P. W. M. Blom, D. M. de Leeuw and B. de Boer, *Adv. Mater.*, 2010, **22,** 933-945.
33 J. F. Scott, Ferroelectric Memories, Springer-Verlag, Berlin 2000.
34 H. S. Lee, S. W. Min, M. K. Park, Y. T. Lee, P. J. Jeon, J. H. Kim, S. Ryu and S. Im, *Small*, 2012, **8,** 3111-3115.
35 S. K. Hwang, S. Y. Min, I. Bae, S. M. Cho, K. L. Kim,T. W. Lee and C. Park, *Small*, 2014, **10,** 1976-1984.
36 Y. Zheng, G. X. Ni, C. T. Toh, M. G. Zeng, S. T. Chen, K. Yao and B. Ozyilmaz, *Appl. Phys. Lett.*, 2009, **94,** 163505.
37 J. Y. Son, S. Ryu, Y. C. Park, Y. T. Lim, Y. S. Shin, Y. H. Shin and H. M. Jang, *ACS Nano*, 2010, **4,** 7315-7320.

38 L. J. Liang, T. Fukushima, K. Nakamura, S. Uemura, T. Kamata and N. Kobayashi, *J. Mater. Chem. C*, 2014, **2,** 879-883.
39 S. E. Shim, Y. J. Cha, J. M. Byun and S. Choe, *J. Appl. Polym. Sci.*, 1999, **71,** 2259-2269.
40 C. Geng, L. Zheng, J. Yu, Q. F. Yan, T. B. Wei, X. Q. Wang and D. Z. Shen, J. Mater. Chem., 2012, **22,** 22678-22685.
41 J. Yu, C. Geng, L. Zheng, Z. H. Ma, T.Y. Tan, X. Q. Wang, Q. F. Yan and D. Z. Shen, *Langmuir*, 2012, **28,** 12681-12689.
42 D. Zhou, K. F. Cheung, Y. Chen, S. T. Lau, Q. F. Zhou, K. K. Shung, H. S. Luo, J. Y. Dai and H. L. W. Chan, *IEEE Trans. Ultrason. Ferroelectr. Freq. Control,* 2011, **58,** 477-484.
43 Y. Zhang, G. Y. Gao, H. L. W. Chan, J. Y. Dai, Y. Wang and J. H. Hao, *Adv. Mater.*, 2012, **24,** 1729-1735.
44 D. B. Lin, Z. R. Li, S. J. Zhang, Z. Xu and X. Yao, J. Appl. Phys., 2010, **108,** 034112.
45 D. Viehland and J. F. Li, *J. Appl. Phys.*, 2001, **90,** 2995-3003.
46 Y. Matsuo, T. Ijichi, J. Hatori, S. Ikehata, *Curr. Appl. Phys.*, 2004, **4,** 210-212.

Nanoscale Accepted Manuscript